Theoretical analysis of the adsorption properties of methyl violet dye on iron-doped mesoporous silica microspheres

Yuan Cao*, Junxia Zhao, Ping Li

College of Chemistry and Chemical Engineering, Chongqing University, Chongqing 400044, China, Tel. +86 15923344273; Fax: +86 23 65111748; email: caoyuan@cqu.edu.cn (Y. Cao)

ABSTRACT

The optimum adsorption conditions of methyl violet (MV) dye from aqueous solutions by iron-doped mesoporous silica microspheres (Fe-MSM) were investigated through adsorption experiments to improve the effect of advanced treatment of dye wastewater. The novel adsorbents were characterized by X-ray diffraction, Fourier transform infrared spectroscopy, N_2 adsorption–desorption isotherms, and scanning electron microscopy. The effects of adsorbent dosage, adsorption time, initial dye concentration, and pH on the adsorption performance were analyzed. Given these effects, the kinetics equation, related parameters, and the adsorption mechanisms were obtained. Results indicate that the different Fe contents had a slight influence on the adsorption capacity of the samples. The adsorption efficiency reached 98% for an MV solution with an initial concentration of 50 mg/L, adsorbent dosage of 10 mg, equilibrium time for adsorption of 30 min, and an alkaline pH. The adsorption process followed the pseudo-second-order kinetic model. The intra-particle diffusion of dye molecules into interior surface was achieved through rate-controlled process, and further adsorption mechanisms were involved except for ion exchange. Fe-MSM could be an ideal material for the treatment of dyestuff wastewater because of its relatively high performance and rapid sorption velocity.

Keywords: Adsorption kinetics; Characterization; Fe-MSM; Methyl violet; Theoretical analysis

1. Introduction

Textile, printing, dyeing, and paper industries discharge a considerable amount of dye wastewater into rivers and lakes, thus resulting in environmental and human health threats because of its high amount of colorant, difficulty to biodegrade, and high content of organic pollutants [1]. Methyl violet (MV) belongs to the triphenylmethane group, which is widely used in Gram staining as well as an anti-allergen, bactericide, or pH indicator. Once inhaled or ingested, the compound irritates the respiratory and gastrointestinal tracts and cause inflammation and toxicity in humans and animals [2,3]. Therefore, dye concentration in the wastewaters should be reduced before its release into marine environments.

Various treatment methods, such as physical separation, chemical oxidation, and biodegradation have been widely applied to remove dyes from wastewaters [4–6]. Physical adsorption is a commonly used method for removing dye and controlling the demand for biochemical oxygen because of its efficient and

*Corresponding author.

economical operation [7]. Studies have searched for a suitable adsorbent and determined the mechanisms of dye adsorption. Adsorption on amorphous families of adsorbents, such as activated carbons, cation exchange membranes, resins, and polymer, remove dye effluents effectively [8–11], but often suffer from high-cost production and difficult regeneration. Other natural adsorbents (e.g. clays, sewage sludge, chitosan and agricultural waste) have been used to perform the desired separations [12–14]. Mesoporous materials are appropriate adsorbents to remove dyes from wastewater because of their unique pore structure. In addition, mesoporous silica microspheres possess ordered and adjustable pore sizes, as well as Si–O and Si–OH groups of adsorbing polar compounds [15]. The microspheres are used to adsorb basic dyes from wastewater.

In a previous study, the potential of Fe-doped zeolite Y on the degradation of Azo dye under different conditions has been demonstrated [16]. Mesoporous materials are expected to be more favorable due to higher surface and pore volume for adsorption. In the present study, iron-doped mesoporous silica microspheres (Fe-MSM) were used as adsorbents to remove MV dyes from aqueous solutions. The effects of adsorbent dosage, initial dye concentration, contact time, and pH on MV adsorption were examined. In addition, adsorption kinetics and the corresponding mechanisms were explored.

2. Materials and methods

2.1. Fe-MSM preparation

Three mesoporous Fe-MSM powders were synthesized in classical alkaline medium by hydration. Subsequently, 3.0 g of cetyl trimethylammonium bromide was added to a mixture of 360 mL of ethanol and 270 mL of distilled water and stirred until clear at room temperature. Following the addition of bromide, x g of $FeSO_4$ ($x = 0.1$, 0.3, and 0.5), 4.2 mL of ammonia, and 17.4 mL of tetraethyl orthosilicate were added to the mixture under stirring. The obtained solution was then stirred for 0.5 min and allowed to stand for 12 h at room temperature. The powder was filtered, washed with ethanol and distilled water, and dried before calcination in a furnace at 550℃ for 6 h to decompose the surfactant. Finally, the mesoporous powders were designated 0.1, 0.3, and 0.5Fe-MSM.

2.2. Characterization

The phase structure of the samples was evaluated using Shimadzu XRD 6000 diffractometer equipped

with a Cu Kα radiation source. Fourier transform infrared (FT-IR) spectra in KBr discs were recorded using a MagnaIR 550I (Nicolet Co., USA) IR spectrophotometer from 4,000 to 400 cm^{-1}. The characteristics of the porous structure, such as surface area and pore volume, were obtained from nitrogen adsorption isotherms measured at 77 K and relative pressure range of 0–1.0 with micromeritics ASAP 2020 V 3.01 H. Scanning electron microscopy (SEM) images were obtained at operating voltages that vary from 1.0 to 30.0 kV using JSM-64901 LV (FEI Co., Dutch) apparatus.

2.3. Adsorption experiments

Dye adsorption data from water solutions were obtained by a batch technique. For adsorbent dosage experiments, 5–50 mg of samples were added into 100 mL glass bottles that contain 20 mL of MV solution, with an initial concentration of 50 mg/L. The bottles were then stirred for 30 min at room temperature to attain the conditions for adsorption equilibrium. For different initial dye concentration and adsorption time experiments, 20 mg of Fe-MSM was added into each MV solution (50 mL) with initial concentrations that vary from 20 to 110 mg/L. The experiments were carried out at room temperature for adsorption times between 3 and 60 min. For pH experiments, 10 mg of Fe-MSM was added into each dye solution (50 mL) with an initial MV concentration of 50 mg/L. The pH levels of the dye solutions were adjusted from 2.0 to 11.0 using HCl or NaOH solutions. The adjustment was performed prior to the addition of the adsorbent. The experiments were conducted at room temperature for 30 min. At the end of each adsorption period, the adsorbent was separated from the attained solution by centrifugation at 8,000 rpm for 20 min. The residual dye concentration in the supernatant solution was analyzed using T6 New Century UV–vis spectrophotometer (Beijing Pgeneral Co., China) by monitoring the changes in absorbance at the wavelength of maximum absorbance (665 nm). Dye removal efficiency was calculated as follows:

$$\text{Dye removal } (\%) = (1 - A_t/A_0) \times 100\% \qquad (1)$$

where A_t and A_0 are the MV absorbances in the solution at times t and $t = 0$, respectively.

2.4. Adsorption kinetic model

The adsorption of dyes onto porous adsorbents follow three consecutive mass transfer steps, namely, external and intra-particle diffusion, and adsorption.

These processes control the adsorption kinetics. Two kinetics pseudo-first-order and pseudo-second-order models were selected to analyze the potential mechanisms of adsorption and the rate-controlling steps, and to determine the changes in adsorption rate for various initial MV concentrations on Fe-MSM. An intra-particle diffusion model was utilized to investigate the rate-controlling step during adsorption [17].

The pseudo-first-order rate expression is given by

$$\frac{\mathrm{d}q_t}{\mathrm{d}t} = k_1(q_e - q_t) \quad (2)$$

where q_e and q_t (mg/L) are the amounts of dye adsorbed on adsorbent at equilibrium and at time t, respectively; k_1 (min^{-1}) is the constant rate of the pseudo-first-order adsorption. Given the initial conditions $q_t = 0$ at $t = 0$, integration of Eq. (2) provides [18]

$$\ln (q_t e - q_t) = \ln q_e - k_1 \quad (3)$$

The pseudo-second-order kinetic model is expressed as

$$\frac{\mathrm{d}q_t}{\mathrm{d}t} = k_2(q_e - q_t)^2 \quad (4)$$

where k_2 (mg/L min) is the constant rate of the model. Integration of Eq. (4) and linear transformation yields

$$\frac{t}{q_t} = \frac{1}{k_2 q_e^2} + \frac{1}{q_e}t \quad (5)$$

The rate parameter of intra-particle diffusion is defined as follows:

$$q_t = k_{i,p}t^{1/2} \quad (6)$$

where $k_{i,p}$ (mg/L min$^{1/2}$) is the constant rate of intra-particle diffusion. $k_{i,p}$ values under different conditions were calculated from the slopes of the corresponding straight line portions of the curves.

3. Results and discussion

3.1. Characterization of the adsorbents

Fig. 1 shows the XRD patterns of MSM and Fe-MSM samples. The marked diffraction peaks at $2\theta = 2.3°$ and a wide diffraction peak at $2\theta = 4°–6°$, respectively, correspond to reflections at (1 0 0) and (1 1 0), which indicate the ordered hexagonal
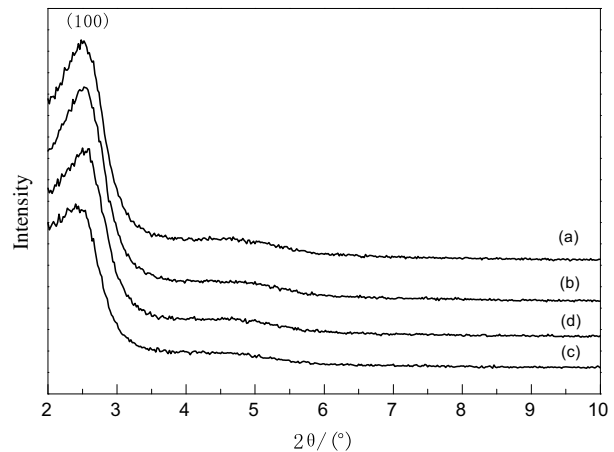

Fig. 1. XRD patterns of (a) MSM; (b) 0.1Fe-MSM; (c) 0.3Fe-MSM; and (d) 0.5Fe-MSM.

structures of the four samples. In addition, the XRD results show that the peak intensities of the three Fe-MSM samples weaken or disappear, indicating that mesoporous materials exhibit low orders after Fe coating [19,20].

Fig. 2 illustrates the FT-IR patterns of the MSM materials, in which the four samples display similar adsorption peaks. The characteristics adsorption peaks observed at 3,439–1,637 cm^{-1} were assigned to stretching vibrations of O–H and bending vibrations of the adsorbed water molecule, respectively. The peaks at 1,086 cm^{-1} are ascribed to symmetric and anti symmetric Si–O–Si stretching vibrations, whereas those between 804 and 417 cm^{-1} correspond to Si–O–Si bending vibrations [21–23]. In addition, the band at 972 cm^{-1} is attributed to the stretching vibrations of Si–O–H and Si–O–Fe, which indicates the successful synthesis of Fe-MSM [24].

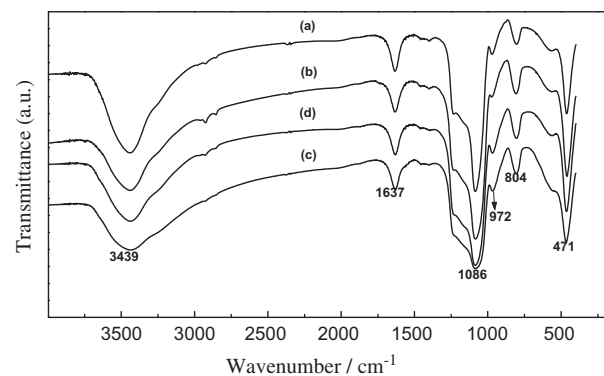The N$_2$ adsorption–desorption isotherms of samples are shown in Fig. 3. The four microsphere

Fig. 2. FT-IR spectra of (a) MSM; (b) 0.1Fe-MSM; (c) 0.3Fe-MSM; and (d) 0.5Fe-MSM.
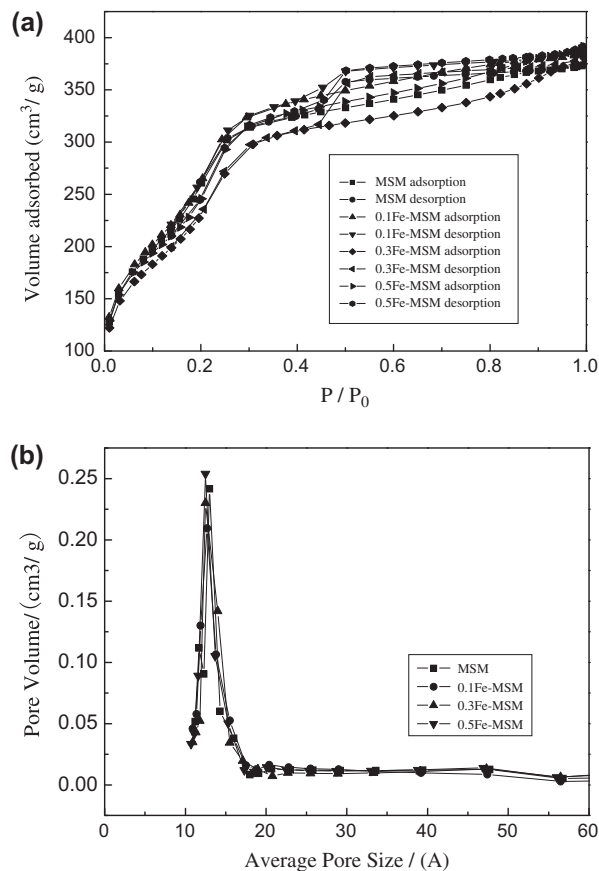
(a)

(b)

Fig. 3. (a) N$_2$ adsorption–desorption isotherm and (b) BJH pore size distribution for MSM, 0.1, 0.3, and 0.5Fe-MSM. P, adsorbate pressure; P_0, saturated vapor pressure of the liquid adsorbate at adsorption temperature of 77 K.

samples exhibit type IV isotherms with a hysteresis loop of type H1, which is attributed to the capillary condensation of nitrogen within mesoporous channels at $P/P^0 = 0.45$–0.80. These results indicate the uniform structures of the mesopores. This observation can be interpreted as a slow rate of increase in N$_2$ uptake at a

low relative pressure, which is associated with the adsorption of the monolayer multilayer on the pore walls [25,26]. The corresponding pore size distribution of Fe-MSM (Fig. 3(b)) was calculated using the Barrett–Joyner–Halenda (BJH) method; results show that the distribution is narrow. Examining the main structural parameters (e.g. pore size, specific surface area, and pore volume; Table 1) reveals that 0.1Fe-MSM has the largest surface area of 982 m^2/g and a relatively high pore volume of 0.59 cm^3/g, which is considered the most important factor related to adsorption performance.

The SEM micrographs of samples are shown in Fig. 4, in which a homogeneous and spherical shape distribution can be observed. The particles for samples A, B, and D are agglomerated because of the physical absorption water. However, the SEM image for sample C was uniform.

3.2. Effect of adsorbent dosage

The percentages of dye removal at different MSM and Fe-MSM doses are shown in Fig. 5. Dye removal was enhanced with increasing adsorbent mass for Fe-MSM contents between 5 and 10 mg because of the increased adsorbent surface area and the availability of more adsorption sites. However, little changes were observed among the dosages between 20 and 50 mg. The rate of MV removal reaches 97–98% when 20 mg of 0.3Fe-MSM and 50 mg of 0.3Fe-MSM were added to the solutions, respectively. The unit adsorption decreased with increasing adsorbent dosage, which can be attributed to the overlap or aggregation of adsorption sites that reduced the total adsorbent surface area available to MV and increased the diffusion path length [27,28]. Fe-MSM demonstrated a higher dye removal rate than MSM at the same adsorbent doses because of the increased active adsorption sites and surface area after Fe loading. Approximately 98, 88, and 97% of the MV were, respectively, adsorbed by

Table 1
Structural parameters of samples

Adsorbent	d_{100}[a] (nm)	a_0[b] (nm)	D[c] (nm)	T[d] (nm)	V[e] (cm^3 g^{-1})	S_{BET} (m^2 g^{-1})
MSM	3.56	4.11	2.36	1.75	0.51	802
0.1Fe-MSM	3.51	4.05	2.41	1.64	0.59	982
0.3Fe-MSM	3.68	4.25	2.77	1.48	0.58	841
0.5Fe-MSM	3.53	4.08	2.65	1.43	0.60	901

[a]Interplanar crystal spacing (1 0 0), $d_{100} = \lambda/2\sin\theta$.
[b]Unit cell parameters, $a_0 = 2d_{100}/\sqrt{3}$.
[c]Average pore size.
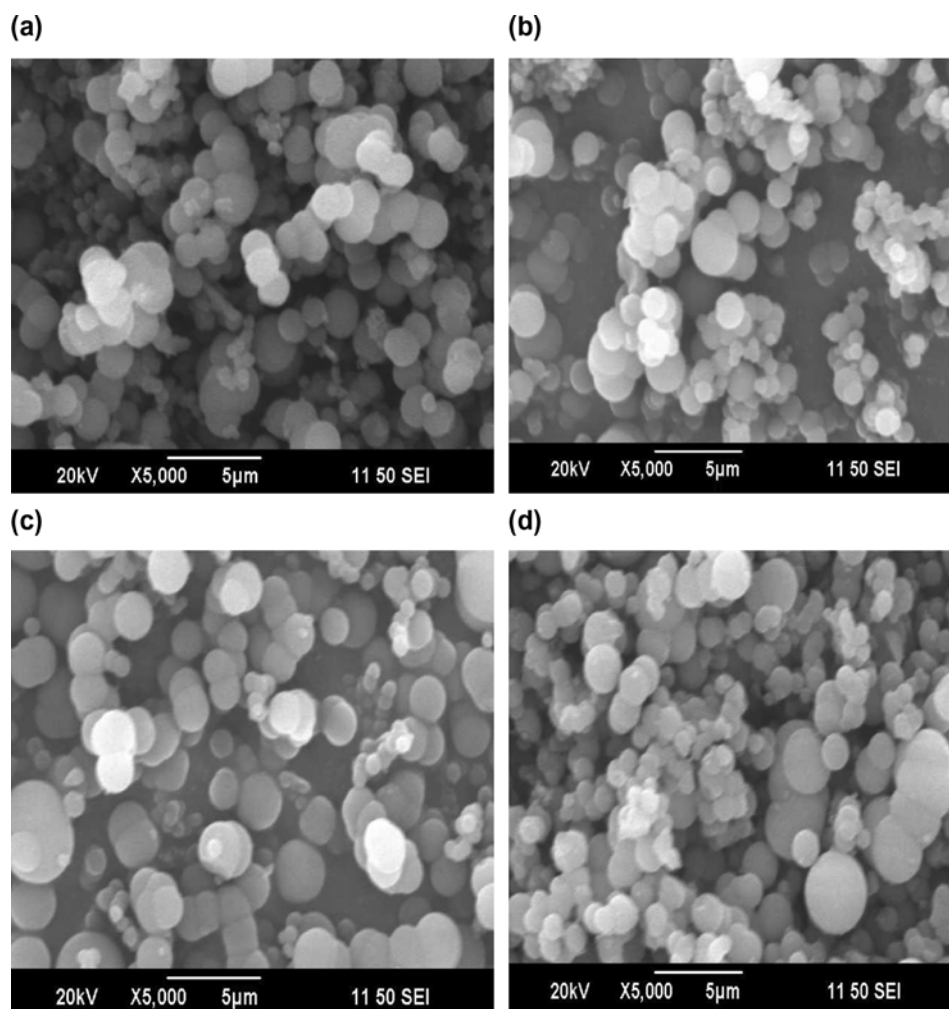[d]Wall thickness, $T = a_0 - D$.
[e]Pore volume.

Fig. 4. SEM photographs of (a) MSM; (b) 0.1Fe-MSM; (c) 0.3Fe-MSM; and (d) 0.5Fe-MSM.
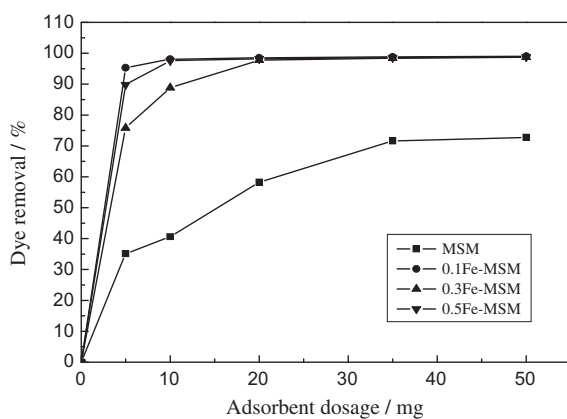

Fig. 5. Effects of various adsorbent dosages on MV removal at an initial MV concentration of 50 mg/L, contact time of 30 min, natural pH, and room temperature.

10 mg of 0.1, 0.3, and 0.5Fe-MSM at an initial MV concentration of 50 mg/L for 30 min. MV uptake reached its maximum for 0.1Fe-MSM, and then decreased with increasing Fe content up to 0.3 g. Finally, the uptake slightly increased for Fe contents beyond 0.3 g. This result implies that increased repulsive forces between the positively charged surface of the adsorbent and MV^+ are predominant for 0.3Fe-MSM adsorption, whereas the increase in ion exchange sites are predominant for 0.5Fe-MSM adsorption. The increase in Fe content, however, slightly affected the adsorption capacity of the samples.

3.3. Effects of initial dye concentration and contact time

As shown in Fig. 6(a)–(c), the adsorption efficiency of Fe-MSM increased along with adsorption time, but decreased with increasing initial dye concentration.
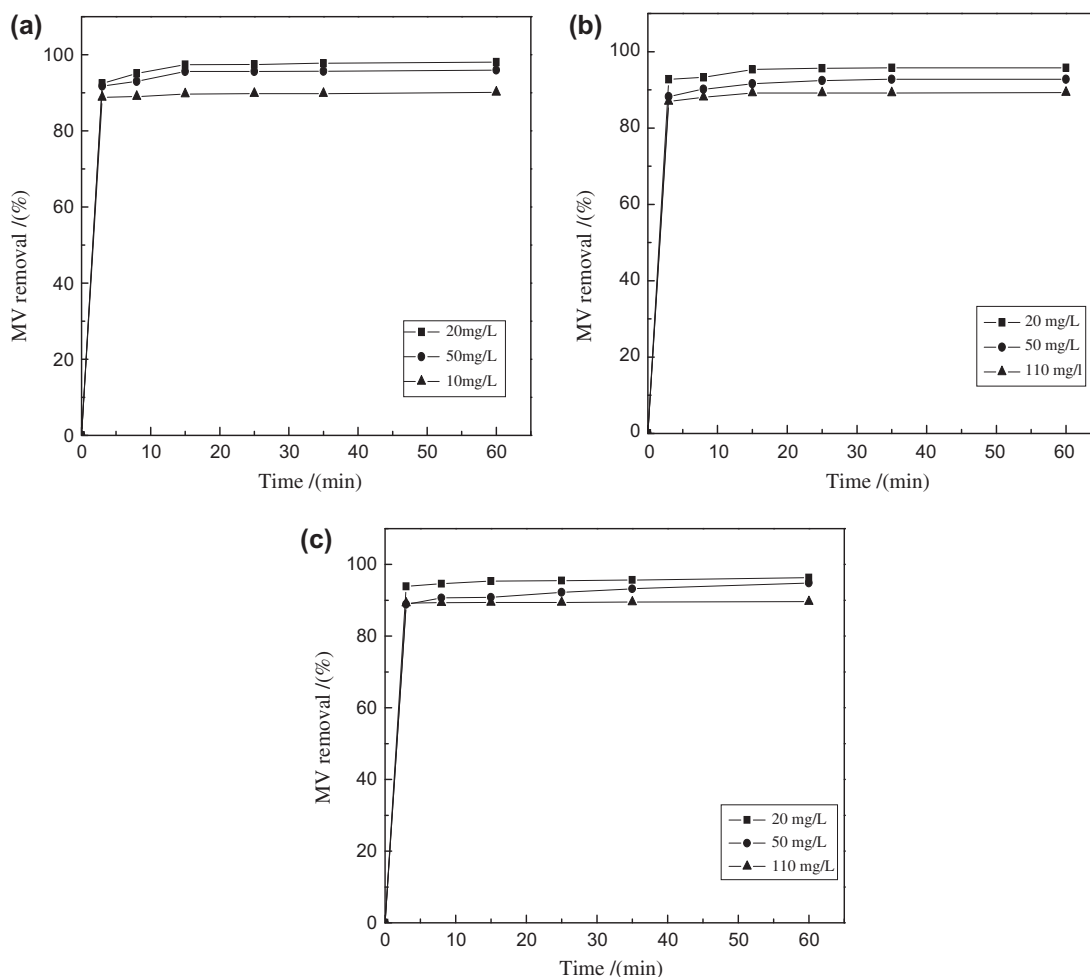
Fig. 6. Effect of adsorbent time on MV removal for an adsorbent dosage of 20 mg, natural pH, and room temperature. (a) 0.1Fe-MSM, (b) 0.3Fe-MSM, and (c) 0.5Fe-MSM.

For example, with increase in the contact time from 3 to 60 min the adsorption rate of 0.1Fe-MSM (initial MV concentration, 20 mg/L) increased from 92.5 to 98.1%. Meanwhile, increasing the initial MV concentration from 20 to 110 mg L^{-1} decreased the MV removal rate of 0.1Fe-MSM (contact time, 60 min) from 98.1 to 90.1% (Fig. 6(a)). The three adsorbents exceed 90% removal within 10 min and almost reached equilibrium for 30 min between the adsorbents and the MV solution. All plots exhibited similar and rapid dye removal rate within the first 5 min, which is followed by a longer period of much slower uptake. Dye molecules rapidly reach the external boundary layer through mass transfer during initial dye adsorption, and slowly diffuse from the exterior surface of the particles into the internal surface. Finally, the molecules diffuse into the porous structure of the adsorbent [29].

3.4. pH effects

The effect of solution pH on the adsorption capacity of Fe-MSM for MV is shown in Fig. 7. The adsorption behavior of the three microsphere samples were similar and significantly affected by pH ranging from 4.0 to 11.0. The adsorption capacity remained almost constant for pH < 5.2. However, the removal of 0.1, 0.3, and 0.5Fe-MSM markedly increased from 76.8, 77.0, and 76.9% at pH 5.2 to 88.4, 92.3, and 90.6% at pH 8.8, respectively. Increasing the pH decreases the charge density of the dye solution, so that the electrostatic repulsion between the positively charged dye molecule and the adsorbent surface is reduced [30]. The lowered electrostatic repulsion increases dye sorption. Similar results have been reported on the adsorption of crystal violet [31,32]. Further increasing the pH
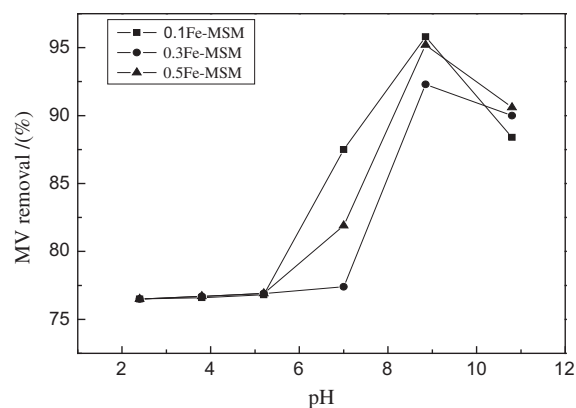
Fig. 7. Effect of pH on MV removal at an initial MV concentration of 50 mg/L, adsorbent dosage of 10 mg, contact time of 30 min, and room temperature.

of the solution (>8.8) decreases the MV uptake to 85%, which is attributed to be destroyed of Fe-MSM hexagonal structure above pH 8.8 [33,34]. Therefore, slightly basic solutions are suitable for removing MV; the maximum MV removal is observed at pH 8.8.

3.5. Adsorption kinetics

The fitting curves of 0.1Fe-MSM for different initial dye concentrations by the pseudo-first-order and pseudo-second-order models are shown in Fig. 8. The pseudo-second-order kinetic model, shown in Fig. 8(a) and (b), exhibits a better linear ($R^2 > 0.99$) than the pseudo-first-order kinetic model. The results indicate that the mechanism of pseudo-second-order adsorption was predominant for MV adsorption onto 0.1Fe-MSM. The equilibrium adsorption capacities (q_e) of 0.1Fe-MSM for 30 min are 19.62, 48, and 99.11 mg/L,

and the rate constants (k_2) are 0.0510, 0.0208, and 0.0101 mg/L min for initial MV concentrations of 20, 50, and 110 mg/L, respectively (Table 2). Moreover, k_2 decreased with increasing initial dye concentration because of the saturation of the adsorption sites at high initial dye concentrations [35]. Furthermore, q_e increased with enhanced initial dye concentration for the three adsorbents, which can be attributed to the efficient utilization of the adsorptive capacities. The latter was induced by the increase in driving force from a high concentration gradient [36].

As shown in Fig. 9, the intra-particle diffusion for adsorption of MV with different initial concentrations onto 0.1Fe-MSM showed both high and low slope linear portions. These observations indicate fast and slow adsorption process; the corresponding intra-particle diffusion rate constants are $k_{i,1}$ and $k_{i,2}$ for various adsorption stages of the exterior and interior surfaces [37]. $k_{i,1}$ and $k_{i,2}$ were found to be 10.68, 26.50, and 56.39 mg/L min$^{1/2}$, and 0.16, 0.39, and 0.27 mg/L min$^{1/2}$ for initial MV concentrations of 20, 50, and 110 mg/L, respectively. The high diffusion rates on the first portion were attributed to the diffusion of dyes from the solution to the exterior adsorbent surface at the onset of the process. $k_{i,1}$ increased with the initial dye concentration. The diffusion of dye molecules through the solution to the surface of adsorbents was affected by the dye concentration owing to the constant agitation speed. The increased dye concentration accelerated dye diffusion because of the increased driving force of the concentration gradient [38,39]. The adsorption into the interior surface of the particles on the second portion is attributed to the saturation of the adsorption of the exterior surface. Therefore, the adsorption rate is very slow, which implies that the intra-particle diffusion of dye molecules into the
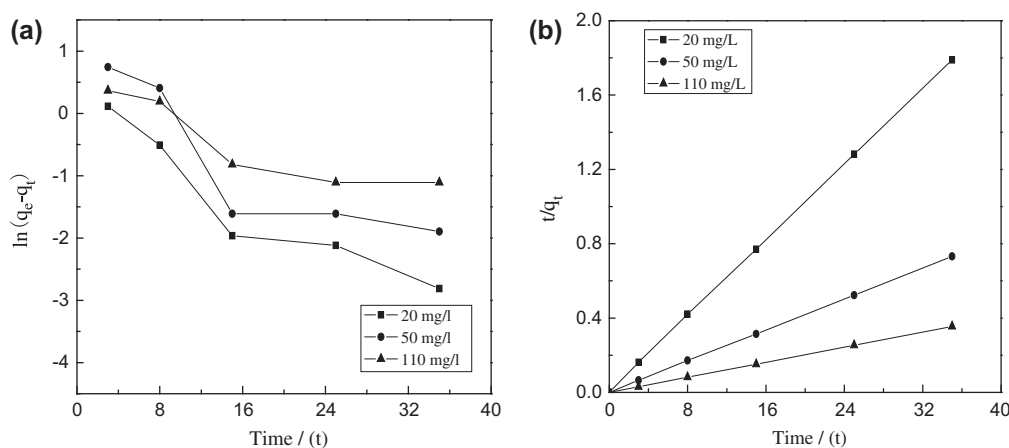

Fig. 8. Fitting of the pseudo-first-order (a) and pseudo-second-order (b) kinetic models for the uptake of 0.1Fe-MSM on MV under different initial concentrations. Conditions: adsorbent dosage, 20 mg; neutral pH; room temperature.

Table 2
Fitting parameters for the uptake of Fe-MSM on MV with various initial concentrations

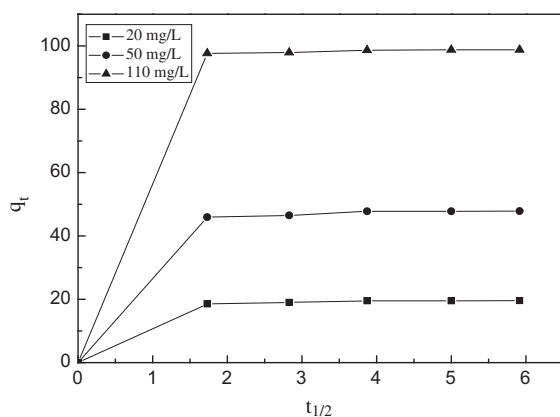| Sample	c_0 (mg/L)	k_2 (mg/L min)	R^2	q_e (mg/L)	k_i (mg/L min$^{1/2}$)	
					Exter $k_{i,1}$	Intra $k_{i,2}$
0.1Fe-MSM	20	0.0510	0.9999	19.62	10.68	0.16
	50	0.0208	0.9999	48	26.50	0.39
	110	0.0101	0.9998	99.11	56.39	0.27
0.3Fe-MSM	20	0.0521	0.9999	19.16	10.71	0.15
	50	0.0215	0.9999	46.4	25.49	0.42
	110	0.0102	0.9998	98.23	55.25	0.35
0.5Fe-MSM	20	0.0522	0.9999	19.26	10.84	0.07
	50	0.0214	0.9999	47.39	25.66	0.44
	110	0.0102	0.9998	98.55	56.65	0.06

Fig. 9. $q_t - t_{1/2}$ for the uptake of 0.1Fe-MSM on MV with different initial concentrations at an adsorbent dosage of 20 mg, neutral pH, and room temperature.

Table 3
$C_{Fe}{}^{3+}$ of the residues in the filtrate after Fe-MSM adsorption

Adsorbent	0.1Fe-MSM	0.3Fe-MSM	0.5Fe-MSM
$C_{Fe}{}^{3+}$ (mg/L)	0.09	0.06	0.07

interior surface was the rate-limiting step during adsorption. Similar kinetic results were found for 0.3 and 0.5Fe-MSM (Table 2).

3.6. Adsorption mechanism analysis

Understanding the mechanisms of MV adsorption on the Fe-MSM surfaces is essential to effectively remove dyes from wastewaters. Aluminum was incorporated into the structures of MCM-41 materials via isomorphous substitution of aluminum for silicon to generate ion exchange sites in mesoporous molecular sieves [40,41]. Therefore, the adsorption of MV onto Fe-MSM is dominated by ion exchange processes. In this study, the ion exchange sites were generated by incorporating Fe into mesoporous silica, and MSM was converted to Fe-MSM. Cationic MV generated exchanges with Fe^{3+} and was adsorbed onto MSM, which resulted to Si–O–MV. Meanwhile, Fe^{3+} remained in the filtrate as residues. The removal rates of 50 mg/L MV by 10 mg of 0.1, 0.3, and 0.5Fe-MSM for 30 min were found to be 96, 92.8, and 94.8%, respectively. The corresponding Fe^{3+} concentrations in the filtrate are shown in Table 3. The results demonstrate that $C_{Fe}{}^{3+}$ in the filtrate is much less than the concentration of adsorbed MV. Therefore, other adsorption processes exist aside from the ion exchange, which is an adsorption mechanism. MV was adequately adsorbed for pH 8.8 because of the formation of hydrogen bonds among silicon hydroxyl groups on the surface of the mesoporous materials and the nitrogen atoms of MV [42] (Fig. 5). Moreover, those adsorption mechanisms may easily induce electron donor or receptor functions between the nitrogen atoms of MV, empty track of Fe-MSM, dispersion forces, and electrostatic interaction [43], as well as increase the adsorption effects.

4. Conclusions

Experiments were performed to investigate and optimize the efficiency of Fe-MSM in removing MV from aqueous solutions under different conditions. The adsorption kinetics and the corresponding mechanisms were analyzed as well. The following observations were drawn based on the results:

(1) Fe-MSM exhibits a much higher adsorption efficiency compared with MSM. However, the increase in Fe content slightly influences the adsorption capacities of the samples. (2) The removal efficiency of Fe-MSM for MV is enhanced with an increase in adsorbent mass and contact time; however, the efficiency decreases with increasing initial dye concentration. Slightly basic solutions (pH 8.8) are suitable for the adsorption of MV on the materials. (3) The pseudo-second-order kinetic model is appropriate for MV adsorption onto Fe-MSM under various initial dye concentrations. Internal diffusion is found to be a rate-controlling process. The adsorption mechanisms involve more than one single ion exchange. The results reveal that Fe-MSM is an efficient adsorbent for the removal of MB from aqueous solutions, as well as to treat colored and effluent water samples.

Acknowledgments

References

[1] C.L. Hsueh, Y.W. Lu, C.C. Hung, Y.H. Huang, C.Y. Chen, Adsorption kinetic, thermodynamic and desorption studies of C.I. Reactive Black 5 on a novel photo assisted Fenton catalyst, Dyes Pigm. 75 (2007) 130–135.

[2] A. Mittal, V. Gajbe, J. Mittal, Removal and recovery of hazardous triphenylmethane dye, methyl violet through adsorption over granulated waste materials, J. Hazard. Mater. 150 (2008) 364–375.

[3] Q. Wu, Z. Shan, M. Shen, S.J. Li, H. Chen, Biosorption of direct scarlet dye on magnetically modified *Saccharomyces cerevisiae* cells, Chin. J. Biotechnol. 25 (2009) 1477–1482.

[4] M. Auta, B.H. Hameed, Coalesced chitosan activated carbon composite for batch and fixed-bed adsorption of cationic and anionic dyes, Colloids Surf., B 105 (2013) 199–206.

[5] S. Senthilkumara, C.A. Bashab, M. Perumalsamya, H.J. Prabhua, Electrochemical oxidation and aerobic biodegradation with isolated bacterial strains for dye wastewater: Combined and integrated approach, Electrochim. Acta 77 (2012) 171–178.

[6] M.M. El-Sheekh, M.M. Gharieb, G.W. Abou-El-Souod, Biodegradation of dyes by some green algae and cyanobacteria, Int. Biodeterior. Biodegrad. 63 (2009) 699–704.

[7] Y. Yao, F. Xu, M. Chen, Z. Xu, Z. Zhu, Adsorption is a comparatively cheap process and effective in the removal of dyes, Bioresour. Technol. 101 (2010) 3040–3046.

[8] S. Azizian, M. Haerifar, H. Bashiri, Adsorption of methyl violet onto granular activated carbon: Equilibrium, kinetics and modeling, Chem. Eng. J. 146 (2009) 36–41.

[9] J.S. Wu, C.H. Liu, K.H. Chu, S.Y. Suen, Removal of cationic dye methyl violet 2B from water by cation exchange membranes, J. Membr. Sci. 309 (2008) 239–245.

[10] F.A. Ozdemir, B. Demirata, R. Apak, Adsorptive removal of Methylene Blue from simulated dyeing wastewater with melamine–formaldehyde–urea resin, J. Appl. Polym. Sci. 112 (2009) 3442–3448.

[11] G. Crini, Kinetic and equilibrium studies on the removal of cationic dyes from aqueous solution by adsorption onto a cyclodextrin polymer, Dyes Pigm. 77 (2008) 415–426.

[12] S.A. Cárdenas, S.L. Cortez, M.C. Mazón, J.C.M. Gutiérrez, Study of malachite green adsorption by organically modified clay using a batch method, Appl. Surf. Sci. 280 (2013) 74–78.

[13] V.M. Monsalvo, A.F. Mohedano, J.J. Rodriguez, Adsorption of 4-chlorophenol by inexpensive sewage sludge-based adsorbents, Chem. Eng. Res. Des. 90 (2012) 1807–1814.

[14] M.C.S. Reddy, L. Sivaramakrishna, A.v. Reddy, The use of an agricultural waste material, Jujuba seeds for the removal of anionic dye (Congo red) from aqueous medium, J. Hazard. Mater 203–204 (2012) 118–127.

[15] M.A. Al-Ghouti, M.A.M. Khraisheh, S.J. Allen, M.N. Ahmad, The removal of dyes from textile wastewater: A study of the physical characteristics and adsorption mechanisms of diatomaceous earth, J. Environ. Manage. 69 (2003) 229–238.

[16] A.J. Nur, Z.A. Ahmad, Low frequency sonocatalytic degradation of Azo dye in water using Fe-doped zeolite Y catalyst, Ultrason. Sonochem. 21 (2014) 743–753.

[17] Q.D. Qin, J. Ma, K. Liu, Adsorption of anionic dyes on ammonium-functionalized MCM-41, J. Hazard. Mater. 162 (2009) 133–139.

[18] L. Li, S.X. Liu, T. Zhu, Application of activated carbon derived from scrap tires for adsorption of Rhodamine B, J. Environ. Sci. 22 (2010) 1273–1280.

[19] A.O. Dhokte, S.L. Khillare, M.K. Lande, B.R. Arbad, Synthesis, characterization of mesoporous silica materials from waste coal fly ash for the classical Mannich reaction, J. Ind. Eng. Chem. 17 (2011) 742–746.

[20] I. Majchrzak-Kucęba, W. Nowak, Characterization of MCM-41 mesoporous materials derived from polish fly ashes, Int. J. Miner. Process 101 (2011) 100–111.

[21] J.S. Choi, D.J. Kim, S.H. Chang, W.S. Ahn, Catalytic applications of MCM-41 with different pore sizes in selected liquid phase reactions, Appl. Catal. A 254 (2003) 225–237.

[22] D.P. Quintanila, I.D. Hierro, M. Fajardo, Sierra, Mesoporous silica functionalized with 2-mercaptopyridine: Synthesis, characterization and employment for Hg(II) adsorption, Microporous Mesoporous Mater. 89 (2006) 58–68.

[23] C. Lesaint, B. Lebean, C. Marichal, J. Patarin, Synthesis of mesoporous silica materials functionalized with *n*-propyl groups, Microporous Mesoporous Mater. 83 (2005) 76–84.

[24] M. Chatterjee, T. Iwasaki, H. Hayashi, Y. Onodera, T. Ebina, T. Nagase, Characterization of tetrahedral vanadium-containing MCM-41 molecular sieves synthesized at room temperature, Chem. Mater. 11 (1999) 1368–1375.

[25] P. Selvam, S.K. Bhatia, C.G. Sonwane, Recent advances in processing and characterization of periodic mesoporous MCM-41 silicate molecular sieves, Ind. Eng. Chem. Res. 40 (2001) 3237–3261.

[26] R. Xu, W. Pang, J. Yu, Q. Huo, J. Chen, Chemistry of zeolites and related porous materials, Adv. Mater. 20 (2008) 843–845.

[27] V.K. Garg, A. Moirangthem, R. Kumar, R. Gupta, Basic dye (methylene blue) removal from simulated waste water by adsorption using Indian Rosewood Sawdust: Timber industry waste, Dyes Pigm. 63 (2004) 243–250.

[28] A. Shukla, Y.H. Zhang, P. Dubey, J.L. Margrave, S.S. Shukla, The role of sawdust in the removal of unwanted materials from water, J. Hazard. Mater. B 95 (2002) 137–152.

[29] S. Senthilkumaar, P.R. Varadarajan, K. Porkodi, C.V. Subbhuraam, Adsorption of methylene blue onto jute fiber carbon: Kinetics and equilibrium studies, J. Colloid Interface Sci. 284 (2005) 78–82.

[30] Y.H. Lin, X.B. He, G.M. Han, Q.J. Tian, W.Y. Hu, Removal of Crystal Violet from aqueous solution using powdered mycelial biomass of Ceriporia lacerata P2, J. Environ. Sci. 23 (2011) 2055–2062.

[31] R. Ahmad, Studies on adsorption of Crystal Violet dye from aqueous solution onto coniferous pinus bark powder (CPBP), J. Hazard. Mater. 171 (2009) 767–773.

[32] A. Saeed, M. Sharif, M. Iqbal, Application potential of grapefruit peel as dye sorbent: Kinetics, equilibrium and mechanism of crystal violet adsorption, J. Hazard. Mater. 179 (2010) 564–572.

[33] P. Kulamani, G.M. Krushna, K.D. Suresh, Adsorption of toxic metal ion Cr(VI) from aqueous state by TiO$_2$-MCM-41: Equilibrium and kinetic studies, J. Hazard. Mater. 241–242 (2012) 395–403.

[34] X.S. Zhao, G.Q.L. Max, G.J. Miller, Advances in mesoporous molecular sieves, Ind. Eng. Chem. Res. 35 (1996) 2075–2090.

[35] E. Eren, O. Cubuk, H. Ciftci, B. Eren, B. Caglar, Adsorption of basic dye from aqueous solutions by modified sepiolite: Equilibrium, kinetics and thermodynamics study, Desalination 252 (2010) 88–96.

[36] H. Deng, J.J. Lu, G.X. Li, G.L. Zhang, X.G. Wang, Adsorption of methylene blue on adsorbent materials produced from cotton stalk, Chem. Eng. J. 172 (2011) 326–334.

[37] Y. Önal, C. Akmil-Başar, D. Eren, Ç.S. Özdemir, T. Depci, Adsorption kinetics of malachite green onto activated carbon prepared from tunçbilek lignite, J. Hazard. Mater. 128 (2006) 150–157.

[38] M. Özacar, Phosphate adsorption characteristics of alunite to be used as a cement additive, Cem. Concr. Res. 33 (2003) 1583–1587.

[39] D.J. Ju, I.G. Byun, J.J. Park, C.H. Lee, G.H. Ahn, T.J. Park, Biosorption of a reactive dye (Rhodamine-B) from an aqueous solution using dried biomass of activated sludge, Bioresour. Technol. 99 (2008) 7971–7975.

[40] W. Bohlmann, D. Michel, 06-P-17—^{27}AlNMR studies on Al-MCM-41 molecular sieves synthesized with different Si/Al ratios and different aluminum sources, Stud. Surf. Sci. Catal. 135 (2001) 421–426.

[41] M.A. Zanjanchi, S. Asgari, Incorporation of aluminum into the framework of mesoporous MCM-41: The contribution of diffuse reflectance spectroscopy, Solid State Ionics 171 (2004) 277–282.

[42] M.A. Al-Ghouti, J.K. Li, Y. Salamh, N. Al-Laqtah, G. Walker, M.N.M. Ahmad, Adsorption mechanisms of removing heavy metals and dyes from aqueous solution using date pits solid adsorbent, J. Hazard. Mater. 176 (2010) 510–520.

[43] R.K. Xu, S.C. Xiao, J.H. Yuan, A.Z. Zhao, Adsorption of methyl violet from aqueous solutions by the biochars derived from crop residues, Bioresour. Technol. 102 (2011) 10293–10298.